Anionic Effects on Li-Ion Activity and Li-Ion Intercalation Reaction Kinetics in Highly Concentrated Li Salt/Propylene Carbonate Solutions

Yosuke Ugata,[†, ‡] Ryoichi Tatara,[†, §] Ji-young Ock,[†] Jingjun Zhang,[†] Kazuhide Ueno,[†, ‡] Masayoshi Watanabe, [‡] and Kaoru Dokko *[, †, ‡]

[†]Department of Chemistry and Life Science, Yokohama National University, 79-5 Tokiwadai, Hodogaya-ku, Yokohama 240-8501, Japan

[‡]Advanced Chemical Energy Research Center (ACERC), Institute of Advanced Sciences, Yokohama National University, 79-5 Tokiwadai, Hodogaya-ku, Yokohama 240-8501, Japan

[§]Present address: Department of Applied Chemistry, Tokyo University of Science, 1-3 Kagurazaka, Shinjuku, Tokyo 162-8601, Japan

*CORRESPONDING AUTHOR

E-mail: dokko-kaoru-js@ynu.ac.jp (K.D.)

Abstract

Certain highly concentrated electrolytes (HCEs) enhance the charge-transfer reaction rate at the electrode/electrolyte interface in Li-ion batteries. The solvation structure of Li^+ in HCEs significantly affects the electrochemical interfacial reaction kinetics. However, the effects of different anions on these kinetics have not yet been fully understood. Therefore, in this study, we investigated the effects of anionic species on the liquid structure and electrochemical reactions of HCEs composed of various Li salts and propylene carbonate (PC). Raman spectra revealed that both PC and anions were coordinated to Li^+ ions in HCEs and that the concentration of uncoordinated (free) PC changed depending on the anionic species. Consequently, the activity of Li^+ in the electrolyte changed depending on the anionic species. The use of Li salts with weakly Lewis basic anions increased the activity of Li^+ and decreased the concentration of free PC in HCEs. The activity of Li^+ in the electrolyte significantly affected the Li^+ intercalation/deintercalation reaction rate of the $LiCoO_2$ thin-film electrode. Electrochemical impedance spectroscopy revealed that the interfacial reaction rate of $LiCoO_2$ was enhanced in the HCEs with anions having weaker Lewis basicity owing to the higher Li^+ ion activity.

1. Introduction

Electrochemical reactions of lithium-ion batteries (LIBs) occur at the electrode/electrolyte interface and the kinetics of these reactions significantly affect the rate capability of LIBs. The Li^+ ions undergo intercalation and deintercalation at the interface, which involve solvation and desolvation. Ogumi and Abe et al. reported that the desolvation of Li^+ is the rate-determining step of the charge transfer reaction at the electrode/electrolyte interface.[1–4] The activation energy for the interfacial charge transfer reaction is correlated with the interaction between Li^+ ions and the solvent, and thus, weak Li^+–solvent interactions are favorable for reducing the activation barrier at the interface and improving the interfacial reaction rate.[5–7] Furthermore, Xu et al. reported that a solid electrolyte interphase (SEI) layer on the graphite negative electrode surface, which is derived from the reductive decomposition products of the electrolyte, also affects the interfacial kinetics of Li^+ intercalation at the graphite/electrolyte interface.[8,9] Therefore, the electrolyte composition critically affects the interfacial charge transfer kinetics in LIBs.

Highly concentrated electrolyte (HCE) solutions containing over 3 mol dm^{-3} of Li salts have attracted attention recently owing to their unique physicochemical and electrochemical properties such as high thermal and electrochemical stability, unusual Li^+ ion transport processes, and good compatibility with next-generation batteries containing Li anodes.[10–15] The kinetics of Li^+ intercalation reactions at the electrodes are faster in certain HCEs compared to that in conventional electrolytes containing 1 mol dm^{-3} of Li salts.[16–18] Typically, in HCEs with Li-salt concentration above 3 mol dm^{-3}, Li^+ ions coordinate to both solvent molecules and anions to satisfy their coordination number owing to the scarcity of the solvent. We previously reported that the Li^+ coordination structures and physicochemical properties of HCEs are significantly affected by the anion species.[19–21] However, the effects of anion species on the interfacial charge transfer kinetics at the electrode/HCE interface have not yet been fully understood.

In this study, we investigated the anionic effects on the Li^+ solvation structure and electrochemistry of highly concentrated Li salt/propylene carbonate solutions. Li salts with various anions, hexafluorophosphate (PF_6^-), bis(fluorosulfonyl)amide (FSA^-), bis(trifluoromethanesulfonyl)amide

(TFSA$^-$), perchlorate (ClO_4^-), tetrafluoroborate (BF_4^-), and trifluoromethanesulfonate (OTf^-), were used as the electrolyte salts (**Figure 1**). Propylene carbonate (PC) is a polar aprotic solvent with a strong ability to solvate alkali metal ions and can dissolve alkali metal salts at high concentrations. Therefore, Li salt/PC solutions have been widely investigated as model electrolytes for LIBs.[22–30] In this study, we analyzed the liquid structures of HCE solutions using Raman spectroscopy. The activity of Li^+ in HCEs was evaluated using a concentration cell. Finally, we investigated the kinetics of Li^+ intercalation/deintercalation of the $LiCoO_2$ thin-film electrodes using the electrochemical impedance method.

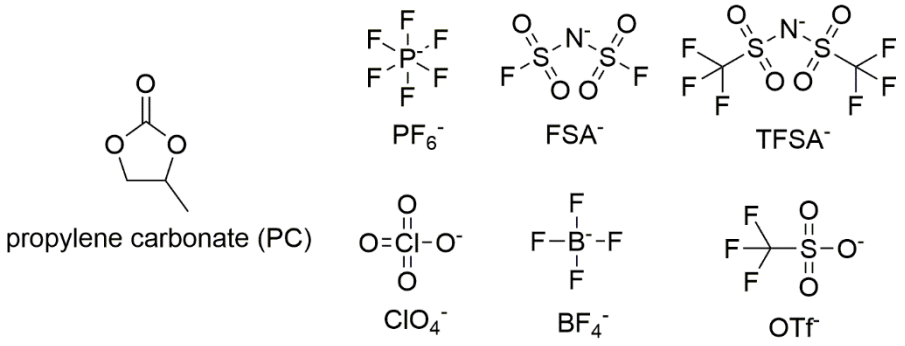

Figure 1. Chemical structures of propylene carbonate and anions of Li salts.

2. Methods

Purified propylene carbonate (PC), battery-grade LiTFSA, LiFSA, $LiPF_6$, $LiBF_4$, and LiOTf were purchased from Kishida Chemical. Battery-grade $LiClO_4$ was purchased from Sigma-Aldrich and was used as received. The electrolyte solutions were prepared by mixing the Li salts and solvents in an Ar-filled glove box (VAC, [H_2O] < 1 ppm). The concentrations of the Li salt in the solutions are summarized in **Tables S1–S6**. The densities and viscosities of the electrolytes (**Tables S7–S10**) were measured using an Anton Paar SVM 3000 viscometer. Raman spectra of the electrolyte solutions were recorded using a JASCO RMP-330 Raman spectrometer with a 532 nm laser. The instrument was

calibrated using a polypropylene standard before the measurements and spectroscopic resolution was 4.5 cm^{-1}. The electrode potentials of the Li metal in the electrolyte solutions were measured using the concentration cell [Li|1 mol dm^{-3} LiTFSA/PC|| *x* mol dm^{-3} Li salt dissolved in PC|Li]. Vycor glass was used as the liquid junction to separate the sample and reference solutions (1 mol dm^{-3} LiTFSA/PC). The electromotive force of the cell at 30 °C was recorded using a Biologic VMP3 electrochemical analyzer.

$LiCoO_2$ thin-film electrodes were prepared using the polyvinylpyrrolidone (PVP) sol-gel method.[31,32] CH_3COOLi (98.0%, Wako Pure Chemical Industries) and PVP (average molecular weight = ~55000, Sigma-Aldrich) were dissolved in a mixture of *i*-C_3H_7OH (99.7%, Wako Pure Chemical Industries) and CH_3COOH (99.7%, Wako Pure Chemical Industries). $Co(CH_3COO)_2 \cdot 4H_2O$ (99.0%, Wako Pure Chemical Industries) was dissolved in purified water. The two solutions were homogeneously mixed to prepare a precursor solution with the final molar ratio of CH_3COOLi:$Co(CH_3COO)\cdot 4H_2O$:PVP:*i*-C_3H_7OH:CH_3COOH:H_2O as 1.1:1:3:10:20:70. The precursor solution was dropped onto the Au substrate and spun at 3000 rpm using a spin coater to obtain a uniform PVP gel film. The gel film was heat-treated in air at 700 °C for 1 h. X-ray diffraction (XRD) patterns of the $LiCoO_2$ thin films were collected using an Rigaku Ultima IV X-ray diffractometer with Cu Kα (λ = 0.154 nm) radiation. The morphology of the thin films was observed using a Hitachi High-Technologies SU8010 scanning electron microscope (SEM).

The electrochemical measurements of the $LiCoO_2$ thin-film electrode were performed using a three-electrode cell. Li metal (Honjo Metal) was employed as both the counter and reference electrodes and a $LiCoO_2$ thin film as the working electrode (electrode area: 1.0 cm^2). Cyclic voltammetry (CV) and electrochemical impedance spectroscopy (EIS) were conducted using a Biologic VSP-300 electrochemical analyzer. Prior to each EIS measurement, the potential of the $LiCoO_2$ electrode was swept to the desired value at a scan rate of 1 mV s^{-1} and held until $LiCoO_2$ reached equilibrium at that potential. The impedance spectra were collected at a given potential in the frequency range of 200 kHz

to 100 mHz with a voltage amplitude of 10 mV root mean square. The cell temperature was controlled using a Espec SU-242 thermostat chamber.

3. Results and Discussion

3.1. Solvation of Li^+ in Li salt/PC mixtures

The liquid structures of the Li salt/PC binary mixtures were investigated by Raman spectroscopy. **Figure 2** shows the Raman spectra of neat PC and Li salt/PC mixtures in the range of 680–780 cm^{-1}. Neat PC exhibits a peak at 712 cm^{-1}, which is attributed to the symmetric ring deformation mode.[24,33–35] When Li salt is added to PC, a new peak appeared at ~722 cm^{-1} corresponding to the PC molecules coordinated to Li^+ ions, i.e., bound PC. However, the quantitative estimation of the amount of uncoordinated (free) and bound PC in the electrolyte using the Raman bands is not possible because of the bands of cis^+ and cis^- conformers of PC overlap.[35] Nevertheless, the Raman band intensities of free and bound PC provide useful information on the liquid structure of the electrolyte. The peak intensity of free PC decreased and that of bound PC increased with increasing Li salt concentration. For HCEs with [Li salt]/[PC] = 1/3 and highly dissociative salts such as $LiPF_6$ and LiFSA, the peak intensity of bound PC is much higher than that of free PC, suggesting that most of the PC molecules are coordinated to Li^+ ions and that free PC molecules hardly exist. In contrast, for HCEs with highly associative salts such as $LiBF_4$ and LiOTf, the peak intensity of free PC is comparable to or greater than that of bound PC, indicating that significant amounts of free PC molecules are present in these solutions. According to literature, the order of ionic association is $LiPF_6$ < LiFSA < LiTFSA ≤ $LiClO_4$ < $LiBF_4$ < LiOTf,[36,37] owing to the respective Lewis basicities of the anions. A strongly Lewis basic anion interacts more strongly with the strongly Lewis acidic Li^+ ion. The Raman spectra in **Figure 2** reveals that the fraction of free PC in the [Li salt]/[PC] = 1/3 HCE increases with increasing attractive interactions between the anion and Li^+.

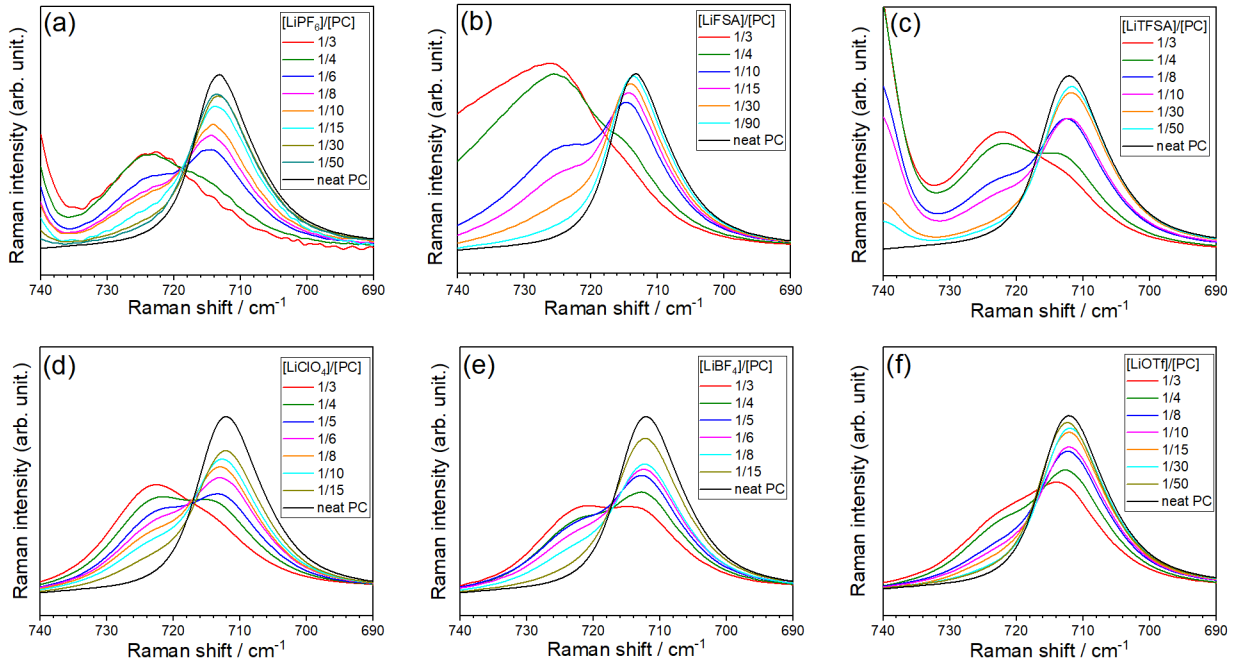

Figure 2. Raman spectra showing the symmetric ring deformation mode of PC in the Li salt/PC mixtures containing (a) $LiPF_6$, (b) LiFSA, (c) LiTFSA, (d) $LiClO_4$, (e) $LiBF_4$, and (f) LiOTf salts at 30 °C.

Figure 3 shows the Raman spectra of the Li salt/PC mixtures corresponding to the vibrational bands of the anions. Each anionic vibrational band is sensitive to the ionic interactions between Li^+ and the corresponding anion in the liquid. For mixtures of $[LiClO_4]/[PC] \leq 1/6$, the Raman band of the symmetric stretching mode of the ClO_4^- anion was observed at ~934 cm^{-1}, which is characteristic of free ClO_4^- and/or ClO_4^- in a solvent-separated ion pair (SSIP);[38–40] this implies that Li^+ ions in mixtures of $[LiClO_4]/[PC] \leq 1/6$ are solvated by PC molecules. With increasing mole fraction of $LiClO_4$ to $[LiClO_4]/[PC] = 1/3$, a shoulder peak at ~940 cm^{-1} became more prominent, suggesting that the ClO_4^- anion directly interacts with a Li^+ ion to form a contact ion pair (CIP).[38–40] Although the Raman bands of anions involved in SSIP and CIP overlap in $LiPF_6$-, LiFSA-, and LiTFSA-based electrolytes,[37,41,42] each band shifts to a higher wavenumber with increasing mole fraction of the Li salt, suggesting that the interactions between Li^+ ions and anions become stronger. In other words, the solvent and the anions are competitively coordinated to Li^+ ions in HCEs irrespective of the anion species. Because the coordination number of Li^+ is typically 4–5 in nonaqueous electrolyte solutions,[34,43] the amount of PC solvent in the

electrolytes with a molar ratio of [Li salt]/[PC] = 1/3 is insufficient to fulfill this coordination number. Therefore, Li^+ ions coordinate to the anions and form CIPs. In the Raman spectra of the mixtures of [$LiBF_4$]/[PC] = 1/3 and [LiOTf]/[PC] = 1/3, intense peaks of BF_4^- and OTf^- appeared at ~775 and ~1050 cm^{-1}, respectively, indicating the formation of ionic aggregates (AGG), in which an anion is coordinated to more than one Li^+ ion.[44–47] This suggests that the more associative anions strongly interact with multiple Li^+ ions and a certain amount of PC is removed from the first solvation sheath of Li^+, resulting in an increase in the fraction of free PC in the electrolyte (*vide supra*).

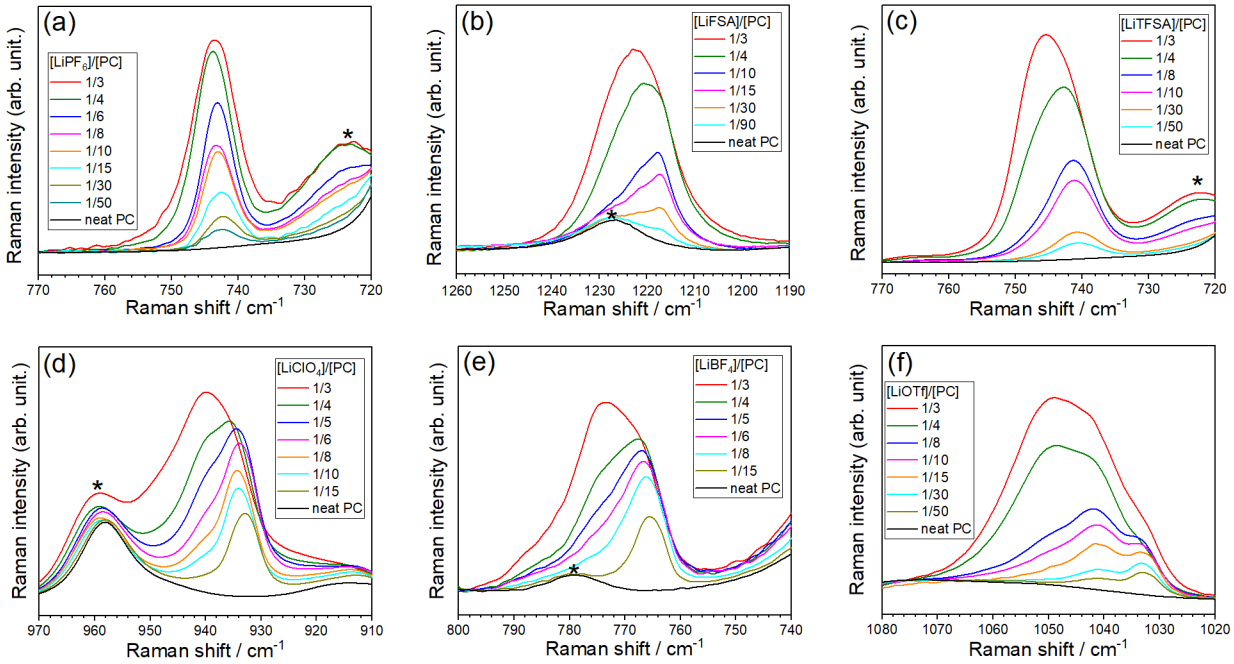

Figure 3. Raman spectra of the vibrational mode of the anions in the Li salt/PC mixtures of (a) $LiPF_6$ (PF_6 symmetric stretching), (b) LiFSA (S=O stretching), (c) LiTFSA (CF_3 bending coupled with S–N stretching), (d) $LiClO_4$ (ClO_4 symmetric stretching), (e) $LiBF_4$ (BF_4 symmetric stretching), and (f) LiOTf (SO_3 symmetric stretching) at 30 °C. The peaks denoted by * at ~ 722, 778, 960, and 1227 cm^{-1} correspond to the symmetric ring deformation, ring deformation, carbonate symmetric stretching vibration, and carbonate asymmetric stretching vibration modes of PC, respectively.[33]

3.2. Electrode potential of Li metal

To evaluate the activities of Li^+ ions in the electrolyte solutions, the electrode potential of the Li metal was measured. During the deposition/dissolution of Li metal, the solvation and desolvation of Li^+

occur at the electrode/electrolyte interface. Therefore, the electrochemical reaction of Li metal in non-aqueous electrolyte solutions can be described as follows:

$$[\mathrm{Li(solvent)}_n]^+ + \mathrm{e}^- \rightleftarrows \mathrm{Li} + n\,\mathrm{solvent} \qquad (1)$$

The Nernst equation for the electrode potential of the reaction in Eq. (1) can be expressed as follows:

$$E = E_1^\circ + \frac{RT}{F}\ln\frac{a_{\mathrm{Li+}}}{a_{\mathrm{solvent}}^n} \qquad (2)$$

where E_1° is the standard electrode potential of Eq. (1), $a_{\mathrm{Li+}}$ and a_{solvent} are the activities of the solvated Li^+ ion and free solvent, respectively, *R* is the gas constant, *T* is the absolute temperature, and *F* is the Faraday constant. The Li deposition/dissolution reactions occur at the Li metal/SEI interface. Even so, the electrode potential of Li metal is determined by the composition of bulk electrolyte solution.[48] **Figure 4** shows the electrode potentials of Li metal in various Li salt/PC electrolytes, measured using a concentration cell. The liquid junction potential in the concentration cell [Li | 1 M LiTFSA/PC || *x* M Li salt/PC | Li] may affect the measured electrode potential of Li metal in the sample solution. The diffusivities of Li^+ and anion in 1 M LiTFSA/PC solution showed similar values (**Table S11**), and Li^+ ion transference number calculated from the diffusivities was 0.41. Therefore, the effect of liquid junction potential was considered to be minor. In dilute electrolyte solutions (≤ 0.1 M) containing excess solvent, the electrode potential of Li metal increased linearly with log c_{Li} irrespective of the anion species (**Figure 4**). This result indicates that the assumption of constant solvent activity (*i.e.*, $a_{\mathrm{solvent}} = 1$) is valid for the dilute electrolytes. The slope of the Li electrode potential vs log c_{Li} in the concentration range 0.01−0.1 M was 50~60 mV per decade irrespective of anionic species, which is in good agreement with the theoretical value (60 mV per decade) for the one-electron reaction. However, for concentrated electrolytes (>1 M and [Li salt]/[PC] > 1/8), the Li electrode potential increased nonlinearly with increasing salt concentration, which is consistent with a previous report on glyme-based HCEs.[15,20,46]

This nonlinear relationship between log c_{Li} and the Li electrode potential can be attributed to the increase in the activity coefficient (γ_{+}) of Li^{+} (where $a_{Li+} = \gamma_{+}c_{Li}$) or a decrease in the activity of the free solvent. Actually, the concentration (or activity) of free solvent decreases with increasing the salt concentration as revealed by Raman spectroscopy (**Figure 2**). However, in the conventional electrolyte solution theory, the activity of solvent is assumed to be unchanged (*i.e.*, $a_{solvent} = 1$) irrespective of salt concentration.[49] If we assume that $a_{solvent}$ is always 1 irrespective of the salt concentration (*i.e.*, neglecting the salt concentration dependency of solvent activity in the electrolyte), the activity coefficient of Li^{+} should increase with c_{Li} at > 1 M Li salt concentrations. The slope of the plot of Li electrode potential vs log c_{Li} varied depending on the anion in the concentration range over 1 M. Here we note that the order of the coordinating ability of anion is related to the strength of ionic association, *i.e.*, $PF_6^{-} < FSA^{-} < TFSA^{-} \leq ClO_4^{-} < BF_4^{-} < OTf^{-}$.[36,37] The electrode potentials in the electrolytes with weakly coordinating anions (PF_6^{-}, FSA^{-}, and $TFSA^{-}$) are higher than those in the electrolytes with strongly coordinating anions (BF_4^{-} and OTf^{-}), suggesting that the activity coefficients of Li^{+} in the concentrated electrolytes with weakly coordinating anions are higher. The strongly coordinating anions preferentially interact with Li^{+} to form CIPs and AGGs in the concentrated electrolytes (**Figure 3**). This might cause the relatively low activity coefficients of Li^{+} in the concentrated electrolytes with strongly coordinating anions.

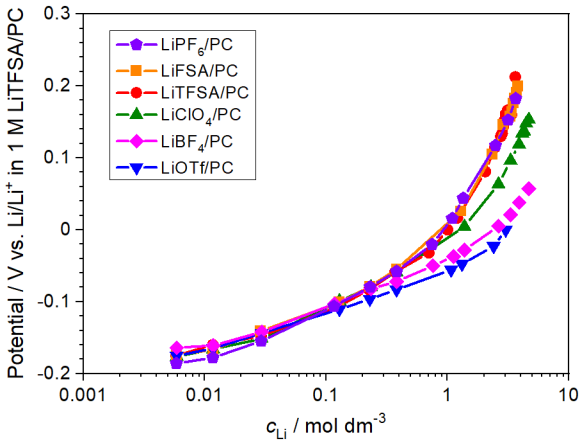

Figure 4. Plots of the Li/Li^+ electrode potential vs Li salt concentration in Li salt/PC mixtures at 30 °C. The reference electrode was Li/Li^+ in 1 mol dm^{-3} LiTFSA/PC.

3.3. Electrochemistry of $LiCoO_2$ thin film

We investigated the effects of the salt concentration and anionic species in the Li salt/PC electrolytes on the electrochemical reactions of $LiCoO_2$ thin-film electrodes. We selected $LiCoO_2$ thin film as the model electrode to avoid the effects of additives such as polymer binders and carbon conductive agents that are often used to fabricate electrodes in LIBs. We prepared the $LiCoO_2$ thin-film electrode via a PVP sol-gel process.[31,50] XRD (**Figure S1**) and Raman spectroscopy (**Figure S2**) confirmed that the prepared $LiCoO_2$ thin film was in a single phase without any impurity phases. The thin film was polycrystalline and comprised submicron-sized grains (**Figure S3**). **Figure 5a** shows the cyclic voltammograms of the $LiCoO_2$ thin-film electrode in the $[LiClO_4]/[PC]$ = 1/10 electrolyte. The main redox peaks were observed at approximately 3.9 V, which is ascribed to Li^+ ion extraction from or insertion into the layered structure of $LiCoO_2$. Two small peaks appeared at 4.07 and 4.17 V, which are attributed to the phase transition between ordered and disordered Li^+ ion arrangements in the CoO_2 framework.[51,52] The peak separation of the main redox peaks at ~3.9 V was small (~40 mV) at a scan rate of 1 mV s^{-1}, which is consistent with previous reports.[32,53] However, upon cycling, the peak separation increased and peak current decreased, indicating cracking of $LiCoO_2$ polycrystalline film occurred during the cycling (*vide infra*). In the case of the cell configuration used in this study (**Figure S4**), no mechanical pressure was applied to the $LiCoO_2$ electrode. Therefore, if cracking of the film occurs during the electrochemical reaction, the electrical contact between the $LiCoO_2$ thin film and Au substrate may partially deteriorate and a certain number of crystal grains might become electrically isolated. This causes increased polarization and capacity loss during cycling.

In the HCE with a molar ratio of $[LiClO_4]/[PC]$ = 1/3, the reversible Li^+ insertion/extraction reactions of $LiCoO_2$ were also observed (**Figure 5b**). The peak separation of the main redox peaks and the peak current density of the voltammogram in the $[LiClO_4]/[PC]$ = 1/3 electrolyte were larger and

lower, respectively, compared with those in the $[LiClO_4]/[PC] = 1/10$ electrolyte. This might be due to the lower ionic conductivity of the former electrolyte (0.58 mS cm^{-1}) than that of the latter one (5.59 mS cm^{-1}). In the case of $[LiClO_4]/[PC] = 1/3$ electrolyte, the deterioration of peak current density upon cycling was suppressed, indicating that the stability of $LiCoO_2$ electrode was improved with increasing the salt concentration. The effect of Li salt concentration on the stability of $LiCoO_2$ electrode will be further discussed later.

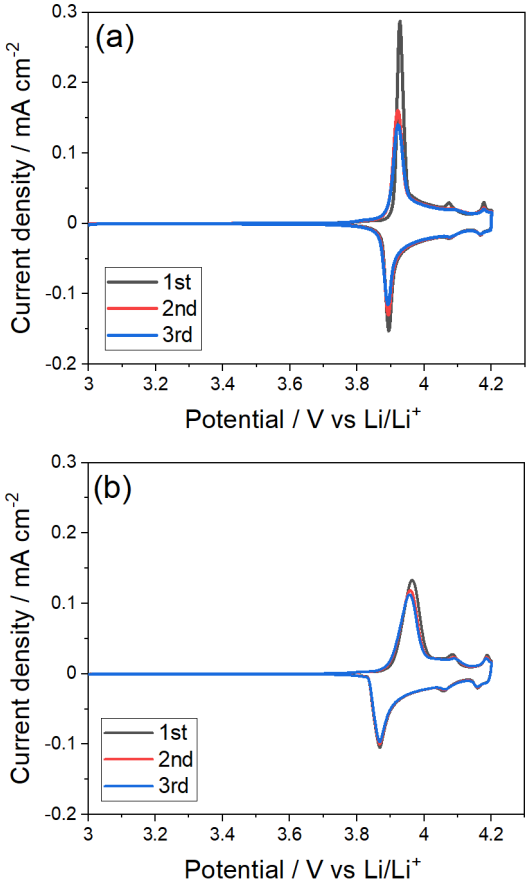

Figure 5. Cyclic voltammograms of $LiCoO_2$ thin-film electrodes in (a) $[LiClO_4]/[PC] = 1/10$ and (b) $[LiClO_4]/[PC] = 1/3$ electrolytes at a scan rate of 1 mV s^{-1} at 30 °C.

To investigate the charge transfer reaction kinetics at the $LiCoO_2$/electrolyte interface, electrochemical impedance spectroscopy (EIS) was performed. **Figure 6** shows Nyquist plots of the $LiCoO_2$ thin-film electrode in the $[LiClO_4]/[PC] = 1/10$ electrolyte at various electrode potentials. A small semicircle is observed in the high-frequency range (> 1 kHz), which did not change with changing

electrode potential and could be attributed to the electronic resistance in the polycrystalline $LiCoO_2$ film and contact resistance between Au and $LiCoO_2$. The thin film exhibited capacitive behavior in the frequency range of < 1 kHz at the open circuit potential of 3.4 V_{Li} (**Figure 6a**) because it becomes a blocking electrode at this potential. When the electrode potential is higher than 3.8 V_{Li}, a second semicircle appeared in the low-frequency region. The diameter of this semicircle changed with changing electrode potential and reached a minimum at 4.0 V_{Li} (**Figure 6b**). Therefore, this semicircle is ascribed to the charge-transfer reaction at the $LiCoO_2$/electrolyte interface. Then, the charge-transfer resistance (R_{ct}) was evaluated by fitting the equivalent circuit shown in the inset of **Figure 6a**, where R_b is the ionic resistance of the bulk electrolyte, R_{HF} is the electronic resistance in the $LiCoO_2$ thin-film, CPEs are the constant phase elements, Z_w is the Warburg impedance**,** and C_L is the Li^+ intercalation capacitance of the thin film.

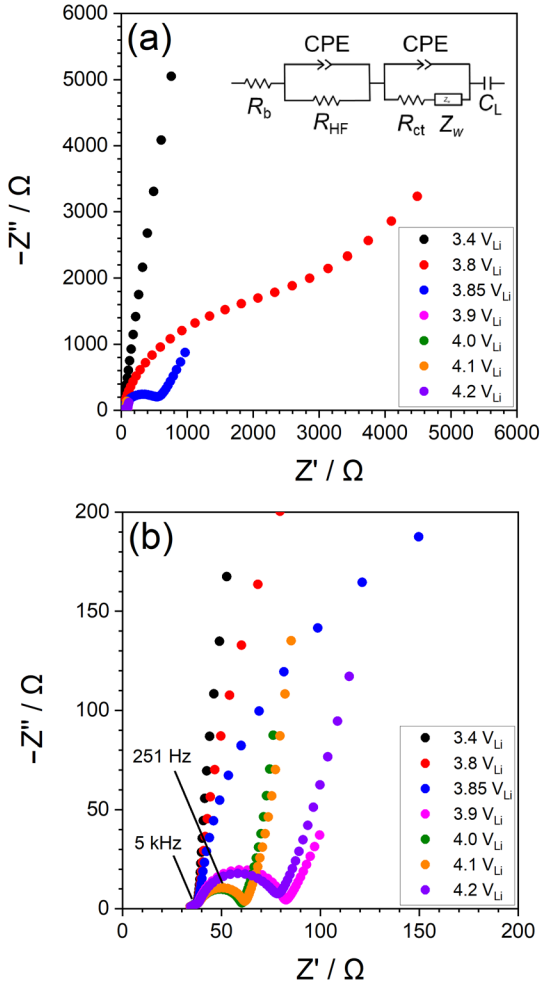

Figure 6. (a) Nyquist plots of $LiCoO_2$ thin-film electrode (area: 1.0 cm^2) in $[LiClO_4]$/[PC] = 1/10 electrolyte at various electrode potentials and 30 °C. (b) Enlarged view of the Nyquist plots.

The temperature dependence of R_{ct} at the $LiCoO_2$/electrolyte interface was also investigated. **Figure 7** shows the Arrhenius plots of T/R_{ct} at the electrode potential of 4.0 V_{Li} in the Li salt/PC electrolytes. R_{ct} was nearly unchanged before and after the temperature-dependent EIS measurements (**Figure S5**). Notably, R_{ct} of the $[LiClO_4]$/[PC] = 1/3 electrolyte was lower than that of the $[LiClO_4]$/[PC] = 1/10 electrolyte in this temperature range. The Li^+ intercalation reaction into the partially delithiated Li_zCoO_2 can be expressed as follows:

$$Li_zCoO_2 + \delta Li^+ + \delta e^- \rightleftarrows Li_{z+\delta}CoO_2 \qquad (3)$$

The exchange current density i_0 for the Li^+ intercalation reaction is inversely proportional to R_{ct} and can be described as follows:[3,54]

$$i_0 = \frac{RT}{FR_{ct}} = k_0 a_{Li+}{}^{(1-\alpha)} a_{solid}{}^{\alpha} \qquad (4)$$

where k_0 is the standard rate constant, a_{solid} is the activity of Li^+ in the partially delithiated $LiCoO_2$, and α is the transfer coefficient ($0 < \alpha < 1$). We can assume that the activity of Li^+ in the partially delithiated $LiCoO_2$ is unchanged during the AC impedance measurement at 4.0 V_{Li}. For simplicity, the Li^+ activity (a_{Li+}) is based on the assumption that the activity of the free solvent is unchanged ($a_{solvent}$ = 1) irrespective of the Li salt concentration (*i.e.*, neglecting the salt concentration dependency of solvent activity in the electrolyte). The transfer coefficient α is typically ~0.5, and Uchimoto et al. reported that the α value is close to 0.5 for the Li^+ intercalation reactions of $Li_xLa_{1/3}NbO_3$ and $LiMn_2O_4$ electrodes.[54–56] Eq. (4) suggests that i_0 increases with increasing Li^+ ion activity (a_{Li+}) (*i.e.*, Li salt concentration) in the electrolyte. The standard rate constant k_0 is expressed as follows:

$$k_0 = A \exp\left(\frac{-\Delta G^*}{RT}\right) \qquad (5)$$

where A is the pre-exponential factor and ΔG^* is the standard Gibbs energy of activation. According to

the literature, the rate-determining step of the Li^+ intercalation reaction is the desolvation process of Li^+ at the electrode/electrolyte interface.[1–4] Therefore, ΔG^* has been assumed to originate mainly from the activation barrier required to break the ion–dipole interaction between Li^+ and the solvent.[5] Assuming that a_{Li+} is unchanged in the measured temperature range, the apparent activation energy E_a(app) of the Li^+ intercalation reaction can be estimated from the Arrhenius plot (**Figure 7a**) using the following equation:

$$\frac{RT}{FR_{ct}} = A' \exp\left(\frac{-E_a(\text{app})}{RT}\right) \qquad (6)$$

where A' is a pre-exponential factor. However, E_a(app) is not equal to ΔG^* (*vide infra*). The E_a(app) value for the $[LiClO_4]$/[PC] = 1/10 electrolyte was estimated as 64 kJ mol^{-1}, which is comparable to a previously reported value.[57] The apparent activation energy estimated from the Arrhenius plot of $1/R_{ct}$ was 62 kJ mol^{-1} (**Figure S6**), which is not significantly different from the value shown in **Figure 7a**. The E_a(app) value for the $[LiClO_4]$/[PC] = 1/3 HCE was estimated as 71 kJ mol^{-1}, which was larger than that for the $[LiClO_4]$/[PC] = 1/10 low-concentration electrolyte (LCE) and is comparable to previously reported values.[58–61] Abe et al. reported an increase in E_a(app) for solid electrolyte/liquid electrolyte[58] and carbonaceous electrode/electrolyte interfaces[59,60] at high salt concentrations in the range of 3–5 M. They speculated that the cleavage of the ion pairs of Li^+-anions at the interface requires a larger ΔG^* than that for the desolvation of Li^+ ions in HCEs.[58] However, here a question arises whether the attractive force between Li^+ and ClO_4^- is stronger than that between Li^+ and PC in the studied electrolytes. Gutmann's donor number (DN) is a good metric of Lewis basicity; the DN of PC is 15.1 kcal mol^{-1},[62] whereas that of ClO_4^- is 8.44 kcal mol^{-1}.[63] As PC is a stronger Lewis base than ClO_4^-, the Lewis acidic Li^+ ions are mainly solvated by PC molecules in the LCEs, as revealed by Raman spectroscopy (**Figure 2**). In HCEs such as $[LiClO_4]$/[PC] = 1/3, both PC and ClO_4^- are coordinated to Li^+ ions. If the complex formation between Li^+ and the anion is the main cause of the increase in E_a(app) in HCEs, E_a(app) is expected to change depending on the anion species. To confirm this hypothesis, we investigated the

temperature dependence of R_{ct} in [Li salt]/[PC] = 1/3 electrolytes containing different Li salts, LiFSA, $LiClO_4$, and LiOTf. As mentioned previously, the coordination ability of the anion increases in the following order: $FSA^- < ClO_4^- < OTf^-$. The DN of OTf^- is 16.9 kcal mol^{-1},[63] which is higher than that of ClO_4^- (8.44 kcal mol^{-1}) and PC (15.1 kcal mol^{-1}). Therefore, the attractive interaction between OTf^- and Li^+ was stronger than that between PC and Li^+. Consequently, OTf^- anions are preferentially coordinated to Li^+, and free PC molecules exist even in HCEs such as [LiOTf]/[PC] = 1/3 (**Figure 2**). **Figure 7b** shows the Arrhenius plot of T/R_{ct} in the [Li salt]/[PC] = 1/3 electrolyte containing different Li salts. R_{ct} values measured at 30 °C were in the order $FSA^- < ClO_4^- < OTf^-$. Because the salt concentrations in the three electrolytes are almost identical (~3 M), the differences in R_{ct} could be attributed to the differences in the activity coefficients of Li^+. As mentioned previously, the activity coefficient of Li^+ is high in HCEs with more weakly coordinating anions. Therefore, the higher activity coefficient of Li^+ in [LiFSA]/[PC] = 1/3 results in a lower R_{ct}, i.e., a higher rate of Li^+ intercalation/deintercalation at the $LiCoO_2$/electrolyte interface. Although R_{ct} value of the [Li salt]/[PC] = 1/3 electrolyte was significantly affected by the anionic species, the E_a(app) values were similar (71–73 kJ mol^{-1}) irrespective of the coordinating ability of the anion, indicating that E_a(app) is not necessarily determined by the interaction strength between Li^+ and the anion in the HCEs.

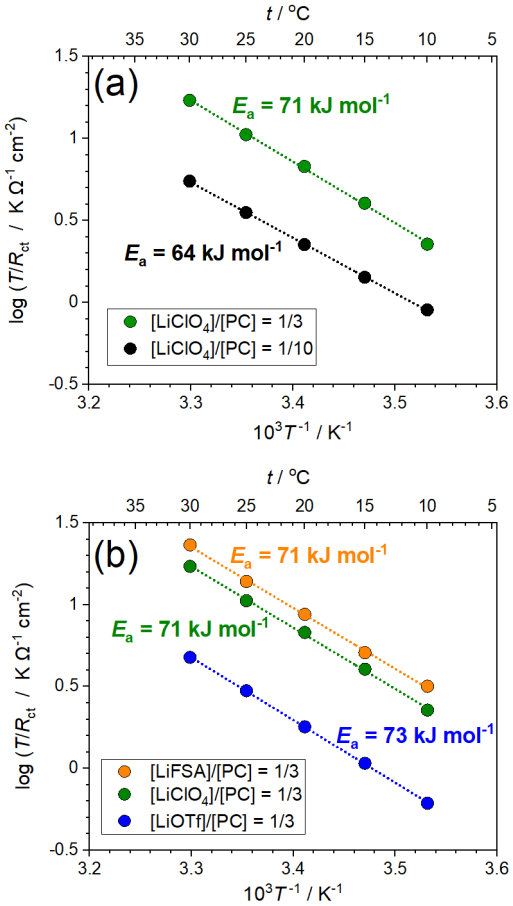

Figure 7. Arrhenius plots of T/R_{ct} for $LiCoO_2$ thin-film electrode at 4.0 V_{Li} in (a) [$LiClO_4$]/[PC] = 1/n (n = 3, 10) and (b) [LiX]/[PC] = 1/3 (X = FSA, ClO_4, OTf) electrolytes.

In addition to the Gibbs energy of activation ΔG^*, the electrolyte viscosity (η) also has a significant effect on the charge-transfer kinetics at the electrode/electrolyte interface. Uchimoto et al. reported a linear relationship between R_{ct} and η for the Li^+ intercalation reaction of $LiMn_2O_4$ at constant temperature.[56] They explained this based on the solvent dynamics theory.[64,65] If the solvent dynamics theory is valid for the Li^+ intercalation reaction, the pre-exponential factor A in Eq. (5) would include the longitudinal relaxation time of the solvent τ_L and is expressed as follows:[66–68]

$$k_0 = \frac{B}{\tau_L}\exp\left(\frac{-\Delta G^*}{RT}\right) \qquad (7)$$

where $B = A\tau_L$. The longitudinal relaxation time τ_L is roughly proportional to η.[64] **Figure 8** shows the Arrhenius plots of the fluidity (reciprocal of viscosity, η^{-1}) of the PC-based LCE and HCEs. LCEs have higher fluidity (i.e., lower viscosity) than that of HCEs. Among the [Li salt]/[PC] = 1/3 HCEs, the LiFSA-

based electrolyte exhibited the highest fluidity (**Figure 8**), which could also explain its high $1/R_{ct}$ (**Figure 7b**). The fluidity of the LiOTf-based electrolyte was higher than that of $LiClO_4$-based one; however, the $1/R_{ct}$ of the former was lower than that of the latter, possibly because of the lower activity coefficient of Li^+ in the former (**Figure 4**). With increasing Li salt concentration, the fluidity of an electrolyte solution decreased, whereas Li^+ activity increased. This tradeoff between a_{Li+} and η^{-1} could provide an electrolyte composition with the maximum $1/R_{ct}$ value. Doi et al. reported that the R_{ct} value at the interface between the NASICON-type Li^+ conductive glass ceramic and $LiBF_4$/PC electrolyte is at its minimum at an electrolyte composition of $[LiBF_4]/[PC] = 1/5$.[61]

Although the temperature dependence of the fluidity of concentrated electrolytes follows the Vogel−Fulcher−Tammann equation over a wide temperature range,[69–71] the fluidity is linearly proportional to $1/T$ in the narrow temperature range of 20–40 °C. The apparent activation energy of fluidity $E_a(\eta^{-1})$ was estimated using the following equation:

$$\eta^{-1} = {\eta_0}^{-1} \exp\left(\frac{-E_a(\eta^{-1})}{RT}\right) \quad (8)$$

where ${\eta_0}^{-1}$ is a pre-exponential factor. As shown in **Figure 8**, the $E_a(\eta^{-1})$ values of the [Li salt]/[PC] = 1/3 HCE are much higher than those of the $[LiClO_4]/[PC] = 1/10$ LCE. Considering the temperature dependence of τ_L, Eq. (7) can be rewritten as follows:

$$k_0 = B{\tau_0}^{-1} \exp\left(\frac{-E_a({\tau_L}^{-1})}{RT}\right) \exp\left(\frac{-\Delta G^*}{RT}\right) \quad (9)$$

where ${\tau_0}^{-1}$ is the pre-exponential factor in the Arrhenius equation of ${\tau_L}^{-1}$ and $E_a({\tau_L}^{-1})$ is the activation energy of ${\tau_L}^{-1}$. Assuming that τ_L is proportional to η in the measured temperature range, $E_a({\tau_L}^{-1})$ is equal to $E_a(\eta^{-1})$. However, the increase in E_a(app) with increasing Li salt concentration from $[LiClO_4]/[PC] = 1/10$ to $[LiClO_4]/[PC] = 1/3$ was only 7 kJ mol^{-1} (**Figure 7a**), whereas the increase in $E_a(\eta^{-1})$ was 31 kJ mol^{-1} (**Figure 8**). This difference might be owing to the temperature dependency of other factors. Previous reports indicate that the association between Li^+ and anions in the electrolyte is enhanced with increasing temperature.[72–74] The enhanced association between Li^+ and anions at high temperatures

lowers the activity coefficient of Li^+ (*vide supra*) and consequently lowers the E_a(app) value. Furthermore, the anion species in the solution affect the temperature dependence of the activity coefficient of Li^+. Consequently, in addition to ΔG^*, the temperature dependence of τ_L and the activity coefficient of Li^+ affect E_a(app) in HCEs.

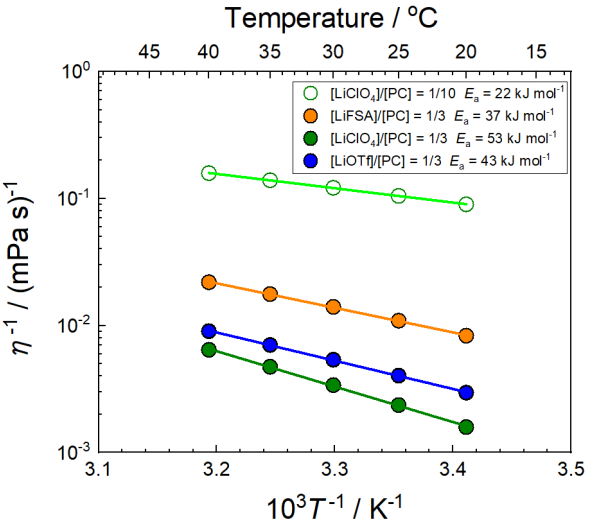

Figure 8. Arrhenius plots of the fluidity (η^{-1}) of the electrolytes with the compositions of [LiFSA]/[PC] = 1/3, [$LiClO_4$]/[PC] = 1/n (n = 3, 10), and [LiOTf]/[PC] = 1/3.

Figure 9a shows the time dependency of the R_{ct} values of $LiCoO_2$ in $LiClO_4$/PC electrolytes at the electrode potential of 4.0 V_{Li}. The R_{ct} value in the [$LiClO_4$]/[PC] = 1/10 electrolyte increased continuously with time. However, this increase is suppressed in the [$LiClO_4$]/[PC] = 1/3 HCE. The surface of the partially delithiated $LiCoO_2$ is more stable and maintains a lower charge transfer resistance in the HCE than in the LCE. Considering the high stability of the crystal structure of $LiCoO_2$ at a potential of 4.0 V_{Li},[51,52] the increase in R_{ct} in the LCE might be related to the chemical and/or electrochemical decomposition of PC molecules on the surface of the partially delithiated $LiCoO_2$ electrode.[75,76] The imaginary part of the impedance ($-Z''$) at the lowest frequency continuously increased with time for 12 h in the [$LiClO_4$]/[PC] = 1/10 electrolyte, which has excess solvent (**Figure S7**). The intercalation capacitance (C_L) of the $LiCoO_2$ thin-film electrode decreased gradually in the [$LiClO_4$]/[PC] = 1/10 electrolyte (**Figure 9b**), whereas that for [$LiClO_4$]/[PC] = 1/3 electrolyte was small. The decrease in C_L

in the former case could be attributed to the cracking of the $LiCoO_2$ thin film electrode. Previous studies reported that the polycrystalline particles in $LiNi_{1-x-y}Mn_xCo_yO_2$ (NMC) positive electrode cracked during charge-discharge cycling; the NMC material has a layered rock salt structure similar to that of $LiCoO_2$.[77–79] In particular, cracking was severe in carbonate-based electrolytes containing excess solvent. Therefore, the cracking was considered to be related to the side reaction of carbonate solvents on the surface of NMC particles. Similarly, the decomposition of the PC solvent might cause the $LiCoO_2$ thin-film electrode to crack in the $[LiClO_4]$/[PC] = 1/10 electrolyte, resulting in a decrease in C_L and an increase in R_{ct}. In the $[LiClO_4]$/[PC] = 1/3 electrolyte, a large fraction of PC was coordinated to Li^+ and the concentration of free PC was extremely low (**Figure 2**). According to previous studies, the solvent coordinated to Li^+ ions is more stable against chemical and electrochemical oxidation at the electrode surface than the free solvent.[80–84] Indeed, the anodic limit of the $LiClO_4$/PC electrolyte solution shifted to a more positive potential as the molar ratio of PC decreased (**Figure S8**). The enhanced oxidative stability of the coordinated PC and the low concentration of free PC in the $[LiClO_4]$/[PC] = 1/3 electrolyte may be effective in suppressing the decomposition of PC, resulting in the suppression of C_L fading and R_{ct} growth.

We further examined the effect of the concentration of free PC on R_{ct} growth and C_L deterioration in HCEs containing different Li salts (**Figures 9c and 9d**). The concentration of the free solvent in HCEs is significantly affected by the Lewis basicity of the anion (**Figure 2**). In the [LiFSA]/[PC] = 1/3 electrolyte with a lower concentration of free PC, the changes in R_{ct} and C_L were small over 12 h. In contrast, in the [LiOTf]/[PC] = 1/3 electrolyte with higher concentrations of free PC, R_{ct} and C_L continuously increased and decreased, respectively, with time. These results demonstrate that the $LiCoO_2$/electrolyte interface can be stabilized by decreasing the concentration of free solvent in the electrolyte.

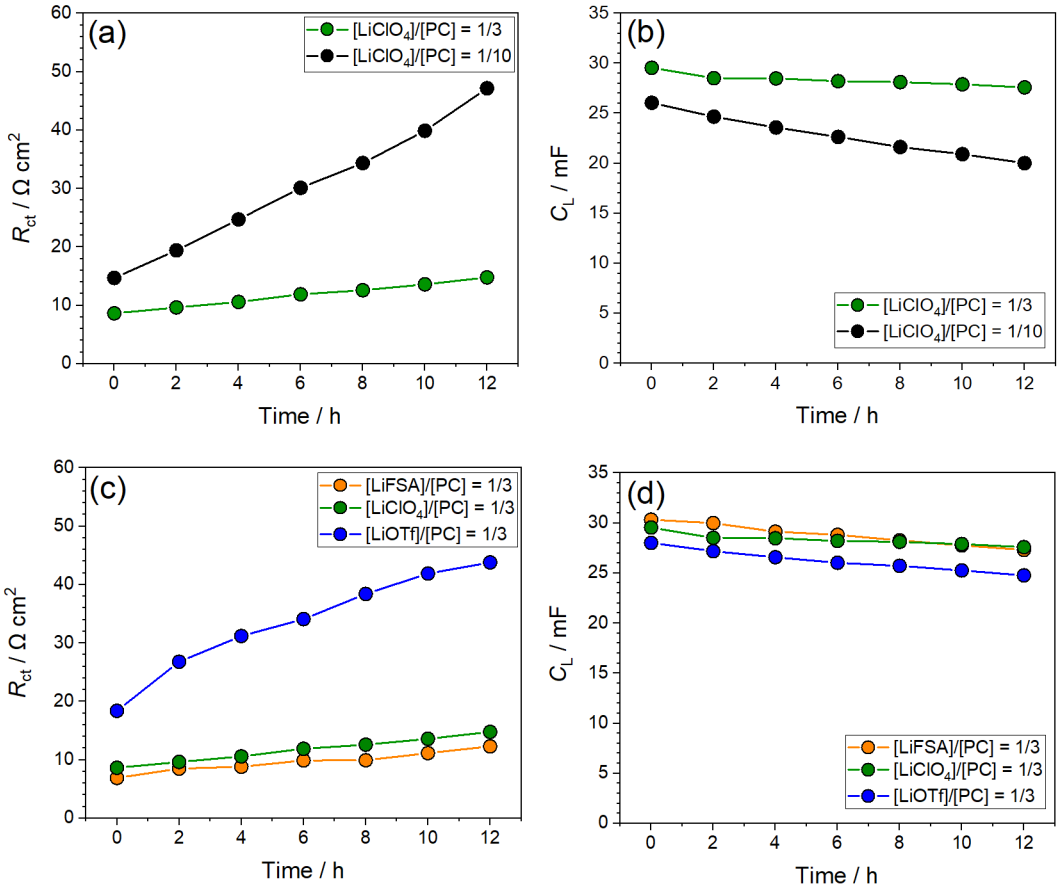

Figure 9. Time dependency of the charge transfer resistance (R_{ct}) and Li^+ intercalation capacitance (C_L) of $LiCoO_2$ thin-film electrodes in (a, b) [$LiClO_4$]/[PC] = 1/n (n = 3, 10) and (c, d) [LiX]/[PC] = 1/3 (X = FSA, ClO_4, OTf) electrolytes measured at 30 °C. The electrode potential of $LiCoO_2$ was set to 4.0 V_{Li}.

4. Conclusions

We investigated the effect of the Lewis basicity of the anion on the interfacial charge-transfer kinetics of $LiCoO_2$ thin-film electrodes in Li salt/PC HCEs. With decreasing Lewis basicity of the anion in HCEs, the ionic association between Li^+ and the anion weakened and the concentration of free PC decreased, resulting in a higher activity coefficient of Li^+. Electrochemical impedance spectroscopy revealed that the charge-transfer resistance at the $LiCoO_2$/electrolyte interface (R_{ct}) decreased as the Li^+ ion activity in the electrolyte increased. Consequently, the use of highly dissociative Li salts with anions having weak Lewis basicity in HCEs is favorable for achieving fast charge-transfer kinetics at the

$LiCoO_2$/electrolyte interface. Furthermore, the concentration of free PC affected the stability of the partially delithiated $LiCoO_2$ electrode in the electrolyte. R_{ct} and Li^+ intercalation capacitance (C_L) of the partially delithiated $LiCoO_2$ electrode increased and decreased, respectively, with time in the electrolytes containing higher concentrations of free PC, whereas R_{ct} growth and C_L fading slowed down in the electrolytes with lower concentrations of free PC. Therefore, the stability of the $LiCoO_2$ electrode can be improved using HCEs with anions having weak Lewis basicity.

ASSOCIATED CONTENT

Supporting Information.

Supporting Information is available free of charge at XXXXX.

Concentrations of Li salts and Li electrode potentials in the electrolytes. Temperature dependence of viscosity, density, and concentration of Li salt in the electrolytes. Diffusivities of ions in 1 M LiTFSA/PC solution. XRD, Raman spectrum, and SEM images of $LiCoO_2$ thin film. Illustration of three electrode cell. Nyquist plots of $LiCoO_2$ thin-film electrode. Arrhenius plots of R_{ct} for $LiCoO_2$ thin-film electrode. Linear sweep voltammograms of electrolytes.

AUTHOR INFORMATION

Corresponding Author

E-mail: dokko-kaoru-js@ynu.ac.jp (K.D.)

Notes

The authors declare no conflicts of interest.

ACKNOWLEDGEMENTS

This study was partially supported by JSPS KAKENHI (Grant No. JP19H05813, JP21H04697, JP22H00340, and JP20J20165) from the Japan Society for the Promotion of Science (JSPS).

References

(1) Abe, T.; Fukuda, H.; Iriyama, Y.; Ogumi, Z. Solvated Li-Ion Transfer at Interface Between Graphite and Electrolyte. *J. Electrochem. Soc.* **2004**, *151*, A1120.

(2) Doi, T.; Iriyama, Y.; Abe, T.; Ogumi, Z. Pulse Voltammetric and Ac Impedance Spectroscopic Studies on Lithium Ion Transfer at an Electrolyte/$Li_{4/3}Ti_{5/3}O_4$ Electrode. *Anal. Chem.* **2005**, *77*, 1696–1700.

(3) Yamada, I.; Iriyama, Y.; Abe, T.; Ogumi, Z. Lithium-Ion Transfer on a $LixCoO_2$ Thin Film Electrode Prepared by Pulsed Laser Deposition-Effect of Orientation-. *J. Power Sources* **2007**, *172*, 933–937.

(4) Kondo, Y.; Abe, T.; Yamada, Y. Kinetics of Interfacial Ion Transfer in Lithium-Ion Batteries: Mechanism Understanding and Improvement Strategies. *ACS Appl. Mater. Interfaces* **2022**, *14*, 22706–22718.

(5) Abe, T.; Sagane, F.; Ohtsuka, M.; Iriyama, Y.; Ogumi, Z. Lithium-Ion Transfer at the Interface Between Lithium-Ion Conductive Ceramic Electrolyte and Liquid Electrolyte-A Key to Enhancing the Rate Capability of Lithium-Ion Batteries. *J. Electrochem. Soc.* **2005**, *152*, A2151.

(6) Yamada, Y.; Iriyama, Y.; Abe, T.; Ogumi, Z. Kinetics of Lithium Ion Transfer at the Interface between Graphite and Liquid Electrolytes: Effects of Solvent and Surface Film. *Langmuir* **2009**, *25*, 12766–12770.

(7) Ishihara, Y.; Miyazaki, K.; Fukutsuka, T.; Abe, T. Kinetics of Lithium-Ion Transfer at the Interface between $Li_4Ti_5O_{12}$ Thin Films and Organic Electrolytes. *ECS Electrochem. Lett.* **2014**, *3*, A83–A86.

(8) Xu, K.; Lam, Y.; Zhang, S. S.; Jow, T. R.; Curtis, T. B. Solvation Sheath of Li^+ in Nonaqueous

Electrolytes and Its Implication of Graphite/Electrolyte Interface Chemistry. *J. Phys. Chem. C* **2007**, *111*, 7411–7421.

(9) Xu, K. "Charge-Transfer" Process at Graphite/Electrolyte Interface and the Solvation Sheath Structure of Li^+ in Nonaqueous Electrolytes. *J. Electrochem. Soc.* **2007**, *154*, A162.

(10) Yamada, Y.; Yamada, A. Review—Superconcentrated Electrolytes for Lithium Batteries. *J. Electrochem. Soc.* **2015**, *162*, A2406–A2423.

(11) Yamada, Y.; Wang, J.; Ko, S.; Watanabe, E.; Yamada, A. Advances and Issues in Developing Salt-Concentrated Battery Electrolytes. *Nat. Energy* **2019**, *4*, 269–280.

(12) Borodin, O.; Self, J.; Persson, K. A.; Wang, C.; Xu, K. Uncharted Waters: Super-Concentrated Electrolytes. *Joule* **2020**, *4*, 69–100.

(13) Li, M.; Wang, C.; Chen, Z.; Xu, K.; Lu, J. New Concepts in Electrolytes. *Chem. Rev.* **2020**, *120*, 6783–6819.

(14) Watanabe, M.; Thomas, M. L.; Zhang, S.; Ueno, K.; Yasuda, T.; Dokko, K. Application of Ionic Liquids to Energy Storage and Conversion Materials and Devices. *Chem. Rev.* **2017**, *117*, 7190–7239.

(15) Ugata, Y.; Shigenobu, K.; Tatara, R.; Ueno, K.; Watanabe, M.; Dokko, K. Solvate Electrolytes for Li and Na Batteries: Structures, Transport Properties, and Electrochemistry. *Phys. Chem. Chem. Phys.* **2021**, *23*, 21419–21436.

(16) Yamada, Y.; Furukawa, K.; Sodeyama, K.; Kikuchi, K.; Yaegashi, M.; Tateyama, Y.; Yamada, A. Unusual Stability of Acetonitrile-Based Superconcentrated Electrolytes for Fast-Charging Lithium-Ion Batteries. *J. Am. Chem. Soc.* **2014**, *136*, 5039–5046.

(17) Petibon, R.; Aiken, C. P.; Ma, L.; Xiong, D.; Dahn, J. R. The Use of Ethyl Acetate as a Sole

Solvent in Highly Concentrated Electrolyte for Li-Ion Batteries. *Electrochim. Acta* **2015**, *154*, 287–293.

(18) Ugata, Y.; Chen, Y.; Sasagawa, S.; Ueno, K.; Watanabe, M.; Mita, H.; Shimura, J.; Nagamine, M.; Dokko, K. Eutectic Electrolytes Composed of $LiN(SO_2F)_2$ and Sulfones for Li-Ion Batteries. *J. Phys. Chem. C* **2022**, *126*, 10024–10034.

(19) Ueno, K.; Yoshida, K.; Tsuchiya, M.; Tachikawa, N.; Dokko, K.; Watanabe, M. Glyme-Lithium Salt Equimolar Molten Mixtures: Concentrated Solutions or Solvate Ionic Liquids? *J. Phys. Chem. B* **2012**, *116*, 11323–11331.

(20) Ueno, K.; Tatara, R.; Tsuzuki, S.; Saito, S.; Doi, H.; Yoshida, K.; Mandai, T.; Matsugami, M.; Umebayashi, Y.; Dokko, K.; Watanabe, M. Li^+ Solvation in Glyme-Li Salt Solvate Ionic Liquids. *Phys. Chem. Chem. Phys.* **2015**, *17*, 8248–8257.

(21) Shigenobu, K.; Shibata, M.; Dokko, K.; Watanabe, M.; Fujii, K.; Ueno, K. Anion Effects on Li Ion Transference Number and Dynamic Ion Correlations in Glyme-Li Salt Equimolar Mixtures. *Phys. Chem. Chem. Phys.* **2021**, *23*, 2622–2629.

(22) Aurbach, D.; Daroux, M. L.; Faguy, P. W.; Yeager, E. Identification of Surface Films Formed on Lithium in Propylene Carbonate Solutions. *J. Electrochem. Soc.* **1987**, *134*, 1611–1620.

(23) Fong, R.; von Sacken, U.; Dahn, J. R. Studies of Lithium Intercalation into Carbons Using Nonaqueous Electrochemical Cells. *J. Electrochem. Soc.* **1990**, *137*, 2009–2013.

(24) Kondo, K.; Sano, M.; Hiwara, A.; Omi, T.; Fujita, M.; Kuwae, A.; Iida, M.; Mogi, K.; Yokoyama, H. Conductivity and Solvation of Li+ Ions of $LiPF_6$ in Propylene Carbonate Solutions. *J. Phys. Chem. B* **2000**, *104*, 5040–5044.

(25) Zhang, S. S.; Xu, K.; Allen, J. L.; Jow, T. R. Effect of Propylene Carbonate on the Low

Temperature Performance of Li-Ion Cells. *J. Power Sources* **2002**, *110*, 216–221.

(26) Jeong, S. K.; Inaba, M.; Iriyama, Y.; Abe, T.; Ogumi, Z. Interfacial Reactions between Graphite Electrodes and Propylene Carbonate-Based Solutions: Electrolyte-Concentration Dependence of Electrochemical Lithium Intercalation Reaction. *J. Power Sources* **2008**, *175*, 540–546.

(27) Nie, M.; Abraham, D. P.; Seo, D. M.; Chen, Y.; Bose, A.; Lucht, B. L. Role of Solution Structure in Solid Electrolyte Interphase Formation on Graphite with $LiPF_6$ in Propylene Carbonate. *J. Phys. Chem. C* **2013**, *117*, 25381–25389.

(28) Takeuchi, M.; Kameda, Y.; Umebayashi, Y.; Ogawa, S.; Sonoda, T.; Ishiguro, S. ichi; Fujita, M.; Sano, M. Ion-Ion Interactions of LiPF6 and LiBF4 in Propylene Carbonate Solutions. *J. Mol. Liq.* **2009**, *148*, 99–108.

(29) Hwang, S.; Kim, D. H.; Shin, J. H.; Jang, J. E.; Ahn, K. H.; Lee, C.; Lee, H. Ionic Conduction and Solution Structure in LiPF6 and LiBF4 Propylene Carbonate Electrolytes. *J. Phys. Chem. C* **2018**, *122*, 19438–19446.

(30) Uchida, S.; Sakaebe, H.; Takeichi, N. Transport Properties of Electrolyte Solution Comprising LiPF6, Ethylene Carbonate, and Propylene Carbonate. *Electrochemistry* **2021**, *89*, 439–446.

(31) Rho, Y. H.; Kanamura, K. Li^+-Ion Diffusion in $LiCoO_2$ Thin Film Prepared by the Poly(Vinylpyrrolidone) Sol-Gel Method. *J. Electrochem. Soc.* **2004**, *151*, A1406.

(32) Matsushita, T.; Dokko, K.; Kanamura, K. Comparison of Electrochemical Behavior of $LiCoO_2$ Thin Films Prepared by Sol-Gel and Sputtering Processes. *J. Electrochem. Soc.* **2005**, *152*, A2229.

(33) Janz, G. J.; Ambrose, J.; Coutts, J. W.; Downey, J. R. Raman Spectrum of Propylene Carbonate. *Spectrochim. Acta Part A Mol. Spectrosc.* **1979**, *35*, 175–179.

(34) Kameda, Y.; Umebayashi, Y.; Takeuchi, M.; Wahab, M. A.; Fukuda, S.; Ishiguro, S.; Sasaki, M.; Amo, Y.; Usuki, T. Solvation Structure of Li^+ in Concentrated $LiPF_6$-Propylene Carbonate Solutions. *J. Phys. Chem. B* **2007**, *111*, 6104–6109.

(35) Allen, J. L.; Borodin, O.; Seo, D. M.; Henderson, W. A. Combined Quantum Chemical/Raman Spectroscopic Analyses of Li+ Cation Solvation: Cyclic Carbonate Solvents - Ethylene Carbonate and Propylene Carbonate. *J. Power Sources* **2014**, *267*, 821–830.

(36) Seo, D. M.; Borodin, O.; Han, S. D.; Ly, Q.; Boyle, P. D.; Henderson, W. A. Electrolyte Solvation and Ionic Association: I. Acetonitrile-Lithium Salt Mixtures: Intermediate and Highly Associated Salts. *J. Electrochem. Soc.* **2012**, *159*, A553–A565.

(37) Han, S.; Borodin, O.; Seo, D. M.; Zhou, Z.; Henderson, W. A. Electrolyte Solvation and Ionic Association V. Acetonitrile-Lithium Bis(Fluorosulfonyl)Imide (LiFSI) Mixtures. *J. Electrochem. Soc.* **2014**, *161*, A2042–A2053.

(38) Grondin, J.; Talaga, D.; Lassègues, J. C.; Henderson, W. A. Raman Study of Crystalline Solvates between Glymes $CH_3(OCH_2CH_2)_nOCH_3$ (n = 1, 2 and 3) and $LiClO_4$. *Phys. Chem. Chem. Phys.* **2004**, *3*, 938–944.

(39) Grondin, J.; Lassègues, J. C.; Chami, M.; Servant, L.; Talaga, D.; Henderson, W. A. Raman Study of Tetraglyme-$LiClO_4$ Solvate Structures. *Phys. Chem. Chem. Phys.* **2004**, *6*, 4260–4267.

(40) Daubert, J. S.; Afroz, T.; Borodin, O.; Seo, D. M.; Boyle, P. D.; Henderson, W. A. Solvate Structures and Computational/Spectroscopic Characterization of $LiClO_4$ Electrolytes. *J. Phys. Chem. C* **2022**, *126*, 14399–14412.

(41) Han, S. D.; Yun, S. H.; Borodin, O.; Seo, D. M.; Sommer, R. D.; Young, V. G.; Henderson, W. A. Solvate Structures and Computational/Spectroscopic Characterization of $LiPF_6$ Electrolytes.

J. Phys. Chem. C **2015**, *119*, 8492–8500.

(42) Henderson, W. A.; Helm, M. L.; Seo, D. M.; Trulove, P. C.; De Long, H. C.; Borodin, O. Electrolyte Solvation and Ionic Association: VIII. Reassessing Raman Spectroscopic Studies of Ion Coordination for LiTFSI. *J. Electrochem. Soc.* **2022**, *169*, 060515.

(43) Hyodo, S.-A.; Okabayashi, K. Raman Intensity Study of Local Structure in Non-Aqueous Electrolyte Solutions—I. Cation-Solvent Interaction in $LiClO_4$/Ethylene Carbonate. *Electrochim. Acta* **1989**, *34*, 1551–1556.

(44) Seo, D. M.; Boyle, P. D.; Allen, J. L.; Han, S. D.; Erlendur, J.; Johansson, P.; Henderson, W. A. Solvate Structures and Computational/Spectroscopic Characterization of $LiBF_4$ Electrolytes. *J. Phys. Chem. C* **2014**, *118*, 18377–18386.

(45) Huang, W.; Frech, R.; Wheeler, R. A. Molecular Structures and Normal Vibrations of $CF_3SO_3^-$ and Its Lithium Ion Pairs and Aggregates. *J. Phys. Chem.* **1994**, *98*, 100–110.

(46) Moon, H.; Tatara, R.; Mandai, T.; Ueno, K.; Yoshida, K.; Tachikawa, N.; Yasuda, T.; Dokko, K.; Watanabe, M. Mechanism of Li Ion Desolvation at the Interface of Graphite Electrode and Glyme-Li Salt Solvate Ionic Liquids. *J. Phys. Chem. C* **2014**, *118*, 20246–20256.

(47) Yun, S.; Han, S.; Borodin, O.; Seo, D. M.; Afroz, T.; Sommer, R. D.; Henderson, W. A. Solvate Structures and Computational/Spectroscopic Characterization of LiCF3SO3 Electrolytes. *J. Phys. Chem. C* **2022**, *126*, 18251–18265.

(48) Ko, S.; Obukata, T.; Shimada, T.; Takenaka, N.; Nakayama, M.; Yamada, A.; Yamada, Y. Electrode Potential Influences the Reversibility of Lithium-Metal Anodes. *Nat. Energy* **2022**, *7*, 1217–1224.

(49) Bockris, J. O. M.; Reddy, A. K. N. *Modern Electrochemistry. Ionics*, 2nd ed.; Springer US: New

York, 1998.

(50) Rho, Y. H.; Kanamura, K. Li^+ Ion Diffusion in $Li_4Ti_5O_{12}$ Thin Film Electrode Prepared by PVP Sol-Gel Method. *J. Solid State Chem.* **2004**, *177*, 2094–2100.

(51) Reimers, J. N.; Dahn, J. R. Electrochemical and In Situ X-Ray Diffraction Studies of Lithium Intercalation in Li_xCoO_2. *J. Electrochem. Soc.* **1992**, *139*, 2091–2097.

(52) Ohzuku, T.; Ueda, A. Solid-State Redox Reactions of $LiCoO_2$ (R3m) for 4 Volt Secondary Lithium Cells. *J. Electrochem. Soc.* **1994**, *141*, 2972–2977.

(53) Rho, Y. H.; Kanamura, K.; Umegaki, T. $LiCoO_2$ and $LiMn_2O_4$ Thin-Film Electrodes for Rechargeable Lithium Batteries. *J. Electrochem. Soc.* **2003**, *150*, A107–A111.

(54) Kobayashi, S.; Uchimoto, Y. Lithium Ion Phase-Transfer Reaction at the Interface between the Lithium Manganese Oxide Electrode and the Nonaqueous Electrolyte. *J. Phys. Chem. B* **2005**, *109*, 13322–13326.

(55) Nakayama, M.; Ikuta, H.; Uchimoto, Y.; Wakihara, M. Study on the AC Impedance Spectroscopy for the Li Insertion Reaction of $Li_xLa_{1/3}NbO_3$ at the Electrode-Electrolyte Interface. *J. Phys. Chem. B* **2003**, *107*, 10603–10607.

(56) Uchimoto, Y.; Amezawa, K.; Furushita, T.; Wakihara, M.; Taniguchi, I. Charge-Transfer Reaction Rate at the $LiMn_2O_4$ Spinel Oxide Cathode/Polymer Electrolyte Interface. *Solid State Ionics* **2005**, *176*, 2377–2381.

(57) Iriyama, Y.; Kurita, H.; Yamada, I.; Abe, T.; Ogumi, Z. Effects of Surface Modification by MgO on Interfacial Reactions of Lithium Cobalt Oxide Thin Film Electrode. *J. Power Sources* **2004**, *137*, 111–116.

(58) Sagane, F.; Abe, T.; Ogumi, Z. Li^+-Ion Transfer through the Interface between Li^+-Ion

Conductive Ceramic Electrolyte and Li^+-Ion-Concentrated Propylene Carbonate Solution. *J. Phys. Chem. C* **2009**, *113*, 20135–20138.

(59) Kondo, Y.; Fukutsuka, T.; Yokoyama, Y.; Miyahara, Y.; Miyazaki, K.; Abe, T. Sodium/Lithium-Ion Transfer Reaction at the Interface between Low-Crystallized Carbon Nanosphere Electrodes and Organic Electrolytes. *ACS Omega* **2021**, *6*, 18737–18744.

(60) Kondo, Y.; Fukutsuka, T.; Yokoyama, Y.; Miyahara, Y.; Miyazaki, K.; Abe, T. Kinetic Properties of Sodium-Ion Transfer at the Interface between Graphitic Materials and Organic Electrolyte Solutions. *J. Appl. Electrochem.* **2021**, *51*, 629–638.

(61) Doi, T.; Oae, H.; Inaba, M. How Is the Concentration Determined for Rapid Lithium Ion Transfer in Highly Concentrated Electrolyte Solutions? *Electrochem. Sci. Adv.* **2022**, *2*, e2100058.

(62) Izutsu, K. *Electrochemistry in Nonaqueous Solutions*, 2nd ed.; Wiley-VCH Verlag GmbH & Co. KGaA: Weinheim, Germany, 2009.

(63) Linert, W.; Camard, A.; Armand, M.; Michot, C. Anions of Low Lewis Basicity for Ionic Solid State Electrolytes. *Coord. Chem. Rev.* **2002**, *226*, 137–141.

(64) Sumi, H.; Marcus, R. A. Dynamical Solvent Effects in Electron Transfer Reactions. *J. Chem. Phys.* **1986**, *84*, 4894–4914.

(65) Maroncelli, M.; Macinnis, J.; Fleming, G. R. Polar Solvent Dynamics and Electron-Transfer Reactions. *Science* **1989**, *243*, 1674–1681.

(66) Bard, A. J.; Faulkner, L. R. *Electrochemical Methods: Fundamentals and Applications, 2nd Edition*; John Wiley & Sons: New York, 2001.

(67) Zhang, X.; Leddy, J.; Bard, A. J. Dependence of Rate Constants of Heterogeneous Electron

Transfer Reactions on Viscosity. *J. Am. Chem. Soc.* **1985**, *107*, 3719–3721.

(68) Harrer, W.; Grampp, G.; Jaenicke, W.; Edangen-niimberg, U. Dependence of the True Rate Constant of Homogeneous Electron Transfer on Solvent Relaxation Time and Viscosity. *J. Electroanal. Chem.* **1986**, *209*, 223–226.

(69) Gu, G. Y.; Bouvier, S.; Wu, C.; Laura, R.; Rzeznik, M.; Abraham, K. M. 2-Methoxyethyl (Methyl) Carbonate-Based Electrolytes for Li-Ion Batteries. *Electrochim. Acta* **2000**, *45*, 3127–3139.

(70) Boisset, A.; Menne, S.; Jacquemin, J.; Balducci, A.; Anouti, M. Deep Eutectic Solvents Based on N-Methylacetamide and a Lithium Salt as Suitable Electrolytes for Lithium-Ion Batteries. *Phys. Chem. Chem. Phys.* **2013**, *15*, 20054–20063.

(71) Yoshida, K.; Tsuchiya, M.; Tachikawa, N.; Dokko, K.; Watanabe, M. Change from Glyme Solutions to Quasi-Ionic Liquids for Binary Mixtures Consisting of Lithium Bis(Trifluoromethanesulfonyl)Amide and Glymes. *J. Phys. Chem. C* **2011**, *115*, 18384–18394.

(72) Stolwijk, N. A.; Kösters, J.; Wiencierz, M.; Schönhoff, M. On the Extraction of Ion Association Data and Transference Numbers from Ionic Diffusivity and Conductivity Data in Polymer Electrolytes. *Electrochim. Acta* **2013**, *102*, 451–458.

(73) Krachkovskiy, S. A.; Bazak, J. D.; Fraser, S.; Halalay, I. C.; Goward, G. R. Determination of Mass Transfer Parameters and Ionic Association of $LiPF_6$: Organic Carbonates Solutions. *J. Electrochem. Soc.* **2017**, *164*, A912–A916.

(74) Ugata, Y.; Hasegawa, G.; Kuwata, N.; Ueno, K.; Watanabe, M.; Dokko, K. Temperature Dependency of Ion Transport in Highly Concentrated Li Salt/Sulfolane Electrolyte Solutions. *J. Phys. Chem. C* **2022**, *126*, 19084–19090.

(75) Kanamura, K.; Toriyama, S.; Shiraishi, S.; Ohashi, M.; Takehara, Z. I. Studies on Electrochemical Oxidation of Non-Aqueous Electrolyte on the $LiCoO_2$ Thin Film Electrode. *J. Electroanal. Chem.* **1996**, *419*, 77–84.

(76) Matsui, M.; Dokko, K.; Kanamura, K. Dynamic Behavior of Surface Film on $LiCoO_2$ Thin Film Electrode. *J. Power Sources* **2008**, *177*, 184–193.

(77) Cao, Z.; Hashinokuchi, M.; Doi, T.; Inaba, M. Improved Cycle Performance of LiNi0.8Co 0.1Mn0.1O2 Positive Electrode Material in Highly Concentrated LiBF4/DMC. *J. Electrochem. Soc.* **2019**, *166*, A82–A88.

(78) Langdon, J.; Cui, Z.; Manthiram, A. Role of Electrolyte in Overcoming the Challenges of LiNiO2 Cathode in Lithium Batteries. *ACS Energy Lett.* **2021**, *6*, 3809–3816.

(79) Wu, F.; Fang, S.; Kuenzel, M.; Mullaliu, A.; Kim, J. K.; Gao, X.; Diemant, T.; Kim, G. T.; Passerini, S. Dual-Anion Ionic Liquid Electrolyte Enables Stable Ni-Rich Cathodes in Lithium-Metal Batteries. *Joule* **2021**, *5*, 2177–2194.

(80) Yoshida, K.; Nakamura, M.; Kazue, Y.; Tachikawa, N.; Tsuzuki, S.; Seki, S.; Dokko, K.; Watanabe, M. Oxidative-Stability Enhancement and Charge Transport Mechanism in Glyme-Lithium Salt Equimolar Complexes. *J. Am. Chem. Soc.* **2011**, *133*, 13121–13129.

(81) Wang, J.; Yamada, Y.; Sodeyama, K.; Chiang, C. H.; Tateyama, Y.; Yamada, A. Superconcentrated Electrolytes for a High-Voltage Lithium-Ion Battery. *Nat. Commun.* **2016**, *7*, 12032.

(82) Doi, T.; Masuhara, R.; Hashinokuchi, M.; Shimizu, Y.; Inaba, M. Concentrated $LiPF_6$/PC Electrolyte Solutions for 5-V $LiNi_{0.5}Mn_{1.5}O_4$ Positive Electrode in Lithium-Ion Batteries. *Electrochim. Acta* **2016**, *209*, 219–224.

(83) Tatara, R.; Yu, Y.; Karayaylali, P.; Chan, A. K.; Zhang, Y.; Jung, R.; Maglia, F.; Giordano, L.; Shao-Horn, Y. Enhanced Cycling Performance of Ni-Rich Positive Electrodes (NMC) in Li-Ion Batteries by Reducing Electrolyte Free-Solvent Activity. *ACS Appl. Mater. Interfaces* **2019**, *11*, 34973–34988.

(84) Zhang, Y.; Katayama, Y.; Tatara, R.; Giordano, L.; Yu, Y.; Fraggedakis, D.; Sun, J. G.; Maglia, F.; Jung, R.; Bazant, M. Z.; Shao-Horn, Y. Revealing Electrolyte Oxidation: Via Carbonate Dehydrogenation on Ni-Based Oxides in Li-Ion Batteries by in Situ Fourier Transform Infrared Spectroscopy. *Energy Environ. Sci.* **2020**, *13*, 183–199.

TOC Graphic